Excitation of Whispering Gallery Magnons in a Magnetic Vortex

K. Schultheiss,[1,*] R. Verba,[2] F. Wehrmann,[1] K. Wagner,[1,3] L. Körber,[1,3] T. Hula,[1,4] T. Hache,[1,5] A. Kákay,[1] A. A. Awad,[6] V. Tiberkevich,[7] A. N. Slavin,[7] J. Fassbender,[1,3] and H. Schultheiss[1,3]

[1]*Helmholtz-Zentrum Dresden–Rossendorf, Institute of Ion Beam Physics and Materials Research, Bautzner Landstraße 400, 01328 Dresden, Germany*

[2]*Institute of Magnetism, National Academy of Sciences of Ukraine, Kyiv 03680, Ukraine*

[3]*Technische Universität Dresden, 01062 Dresden, Germany*

[4]*Westsächsische Hochschule Zwickau, 08056 Zwickau, Germany*

[5]*Institut für Physik, Technische Universität Chemnitz, 09107 Chemnitz, Germany*

[6]*Department of Physics, University of Gothenburg, 412 96 Gothenburg, Sweden*

[7]*Department of Physics, Oakland University, Rochester, Michigan 48309, USA*

(Received 2 September 2018; published 5 March 2019)

We present the generation of whispering gallery magnons with unprecedented high wave vectors via nonlinear 3-magnon scattering in a μm-sized magnetic $Ni_{81}Fe_{19}$ disc which is in the vortex state. These modes exhibit a strong localization at the perimeter of the disc and practically zero amplitude in an extended area around the vortex core. They originate from the splitting of the fundamental radial magnon modes, which can be resonantly excited in a vortex texture by an out-of-plane microwave field. We shed light on the basics of this nonlinear scattering mechanism from an experimental and theoretical point of view. Using Brillouin light scattering microscopy, we investigated the frequency and power dependence of the 3-magnon splitting. The spatially resolved mode profiles give evidence for the localization at the boundaries of the disc and allow for a direct determination of the modes wave number.

DOI: 10.1103/PhysRevLett.122.097202

One of the most fascinating topics in current quantum physics are hybridized systems, in which different quantum resonators are strongly coupled. Prominent examples are circular cavities that allow the coupling of optical whispering gallery modes [1–5] to microwave cavities [6] or magnetic resonances [7–10]. Whispering gallery modes play a special role in this endeavor because of their high quality factor and strong localization, which ultimately increases the overlap of the wave functions of quantum particles in hybridized systems. In optomagnonics the hybridization with magnons, the collective quantum excitations of the electron spins in a magnetically ordered material, is of particular interest because magnons can take over two functionalities: due to their collective nature they are robust and can serve as a quantum memory [11] and, moreover, they can act as a wavelength converter between microwave and terahertz photons [9]. However, the observation of whispering gallery magnons has not yet been achieved due to the lack of efficient excitation schemes for magnons with large wave vectors in a circular geometry. To tackle this problem, we studied nonlinear 3-magnon scattering [12–15] as a means to generate whispering gallery magnons. This Letter discusses the basics of this nonlinear mechanism in a confined, circular geometry from an experimental and theoretical point of view.

Whispering gallery magnons are eigenmodes in systems with rotational symmetry. This not only applies to the geometry of the magnetic element but also to the magnetization texture therein. For that reason, we study a $Ni_{81}Fe_{19}$ disc that inherently exhibits a magnetic vortex structure [16–20]. The red arrows in Fig. 1(a) schematically depict the generic features of such a vortex in a 50-nm thick $Ni_{81}Fe_{19}$ disc with 5.1 μm diameter: the magnetic moments curl in plane along circular lines around the vortex core, a nanoscopic region in the center of the disc where the magnetization tilts out of plane. According to this rotational symmetry, the magnon eigenmodes in a vortex are characterized by mode numbers (n, m), with $n = 0, 1, 2, \ldots$ counting the number of nodes across the disc radius and $m = 0, \pm 1, \pm 2, \ldots$ counting the number of nodes in azimuthal direction over half the disc [21,22].

Other than commonly known waves, like sound, water, or electromagnetic waves, magnons exhibit a strongly anisotropic dispersion relation in in-plane magnetized thin films [23]. In a vortex, this results in increasing (decreasing) mode energies for increasing n (m) as shown by our analytic calculations in Fig. 1(b). An introduction to these calculations is given in the Supplemental Material [24], which includes Refs. [20,22,25–29]. The four exemplary intensity profiles for the eigenmodes (0,0), (0,10), (0,20), and (0,30), that are shown in Fig. 1(c), reveal the character of whispering gallery magnons: the larger m, the more the magnon intensity is pushed toward the perimeter of the disc. This can be understood intuitively by the reduction of

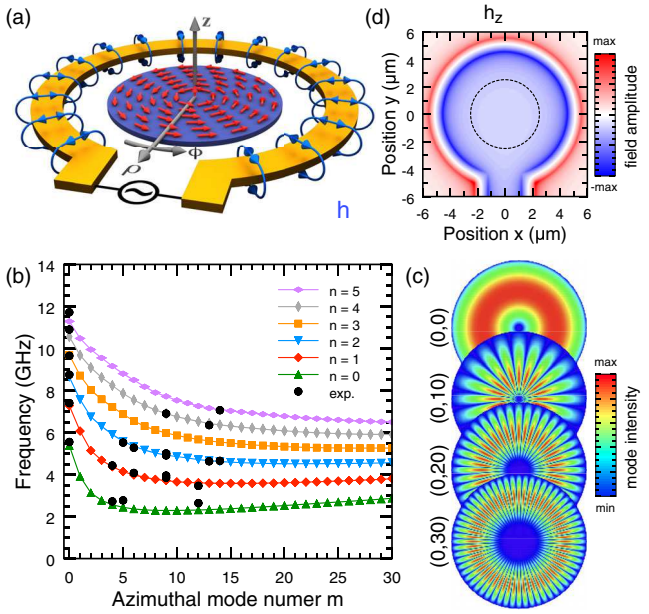

FIG. 1. (a) A $Ni_{81}Fe_{19}$ disc with 50 nm thickness and 5.1 μm diameter is patterned inside an Ω-shaped Au antenna (for fabrication details please see Supplemental Material [24]). Red arrows depict the magnetization configuration of the magnetic vortex structure and the blue lines represent the dynamic magnetic field generated by the loop-shaped microwave antenna. (b) Analytical calculation of the magnon mode frequencies as a function of the radial and azimuthal mode numbers n, m (see Supplemental Material [24]). Black dots show experimental results. (c) Four exemplary mode profiles resulting from analytical calculations. The larger m, the more pronounced the character of the whispering gallery magnons is revealed. (d) COMSOL simulation of the z component of exciting magnetic field **h** generated by the Ω-shaped antenna. The dashed circle indicates the size and position of the disc.

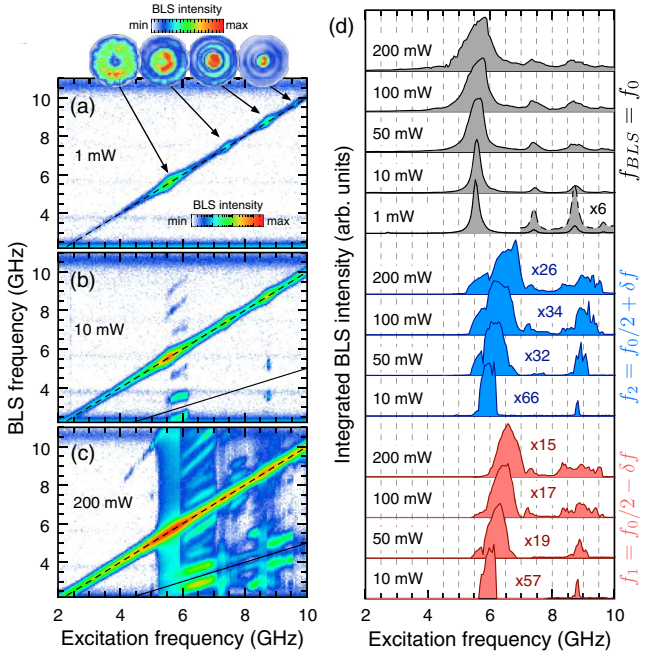

FIG. 2. (a)–(c) BLS spectra for excitation frequencies f_0 between 2 and 10 GHz and excitation powers of 1, 10, and 200 mW, respectively. The diagonal dashed lines indicate the directly excited magnetic oscillations at $f_{\mathrm{BLS}} = f_0$. The solid lines indicate frequencies measured at half the excitation frequency $f_{\mathrm{BLS}} = f_0/2$. At 10 and 200 mW, off-diagonal signals associated with multimagnon scattering processes are detected. (d) Black data show the BLS intensity integrated in 800-MHz wide windows around the direct excitation for 1, 10, 50, 100, and 200 mW (bottom to top). At 1 mW, the intensity integrated for excitation frequencies between 7 and 10 GHz was multiplied by a factor of 6 to better visualize the resonances of the higher order radial modes. Blue (red) data show the intensities of the split modes integrated in 1.4-GHz wide windows around $f_1 = f_0/2 + \delta f$ ($f_2 = f_0/2 - \delta f$) with $\delta f = 800$ MHz.

exchange energy: Leaving an extended area around the vortex core with zero amplitude avoids a strong tilt of neighboring spins close to the vortex core and, therefore, reduces the total energy.

Even though magnon spectra in magnetic vortices have been intensively studied in the past [20,21,30,31], magnons with large azimuthal wave vectors have not yet been measured experimentally and were only observed in micromagnetic simulations [32]. The challenge to generate such magnons and, thereby, to reach out to whispering gallery magnons is finding an efficient excitation mechanism. Here, we tackle this problem via nonlinear 3-magnon scattering. In this process, one magnon splits in two magnons under conservation of energy and momentum. The rotational symmetry of the vortex texture implies specific selection rules for the scattering process which we will describe in context with the experimental data.

In order to selectively excite magnetization dynamics, we apply microwave currents to an Ω-shaped gold antenna that encloses the vortex [Fig. 1(a)]. Inside the Ω loop, a spatially uniform magnetic field is generated that is oriented perpendicularly to the disc as shown in Fig. 1(d). The rotational symmetry of this magnetic field prohibits direct coupling to magnons with $m \neq 0$. However, because of the small diameter of the antenna, strong magnetic fields can be generated so that these magnons can be indirectly excited in the nonlinear regime via multimagnon scattering processes.

We track these nonlinear processes by measuring magnon spectra as a function of the applied microwave frequency using Brillouin light scattering (BLS) microscopy [33]. We would like to emphasize that even though the system is driven with one particular microwave frequency, the BLS technique allows us to detect the dynamic magnetic response in a broad frequency range. In Figs. 2(a)–2(c) we plot the BLS spectra measured between 2 and 11 GHz (y axis) for each excitation frequency (x axis) at microwave powers of 1, 10, and 200 mW. The magnon intensity is encoded using the same logarithmic scale shown as an inset in Fig. 2(a).

At the lowest microwave power of 1 mW [Fig. 2(a)], magnons are excited in the linear regime, which is corroborated by the fact that magnons are only observed at the BLS frequency that matches the applied microwave frequency $f_{\mathrm{BLS}} = f_0$. Hence, the measured intensities strictly follow the diagonal, dashed line. Four distinct resonances emerge at 5.55, 7.40, 8.75, and 9.65 GHz, which we identify as the well-known first four radial modes [21,34] by spatially resolved BLS microscopy [insets in Fig. 2(a)].

At a power of 10 mW [Fig. 2(b)], the excitation field is strong enough to generate magnons in the nonlinear regime. Hence, we observe strong off-diagonal signals that appear at BLS frequencies symmetrically spaced around half the excitation frequency $f_0/2$ (straight line with slope 0.5). These satellite peaks are the result of 3-magnon splitting processes. In order to conserve energy the initial magnon with frequency f_0 splits in two magnons with frequencies $f_1 = f_0/2 - \delta f$ and $f_2 = f_0/2 + \delta f$. Moreover, the rotational symmetry of the vortex requires conservation of the momentum component in azimuthal direction. For an initial magnon with $m = 0$ this implies that the split modes have azimuthal mode numbers with the same modulus but opposite sign: $m_1 = -m_2$. Our analytic calculations further show that the split modes must not share the same radial index, i.e., $n_1 \neq n_2$ (see Supplemental Material [24]). All three selection rules drastically restrict the possible scattering channels within the discrete eigenmode spectrum of the vortex [see Fig. 1(b)].

Besides the magnons with frequencies f_1 and f_2, we observe integer multiples thereof. We attribute these signals to higher harmonics giving evidence to large amplitude resonances with a high q factor.

At the maximum applied microwave power of 200 mW, the number of off-diagonal signals increases further [Fig. 2(c)]. Especially, for excitation frequencies between 6 and 7 GHz, we do not just measure two satellite peaks with frequencies f_1 and f_2 but a total number of ten additional modes. Their presence is attributed to avalanche processes of higher order multimagnon scattering. Their frequencies are given by combinations of the three initial magnons, e.g., $2f_1$, $2f_2$, $f_0 + f_1$. Furthermore, the significant line broadening of the directly excited mode and of the split modes in the frequency range between 5.3 and 5.9 GHz can be attributed to 4-magnon scattering [35]. However, this Letter solely focusses on the study of the initial 3-magnon scattering processes which dominate in intensity due to the lower threshold compared to 4-magnon scattering.

To better illustrate the power dependence of the observed modes, we plot the BLS intensity integrated over different frequency windows as a function of the excitation frequency in Fig. 2(d). The black data resemble the BLS intensity of the direct excitation. With increasing power the initially sharp resonances become broader and show the characteristic nonlinear foldover to higher frequencies [36,37]. The red and blue data in Fig. 2(d) show the intensities of the split modes below (red data) and above $f_0/2$ (blue data), which overall broaden in range and shift to higher frequencies with increasing power.

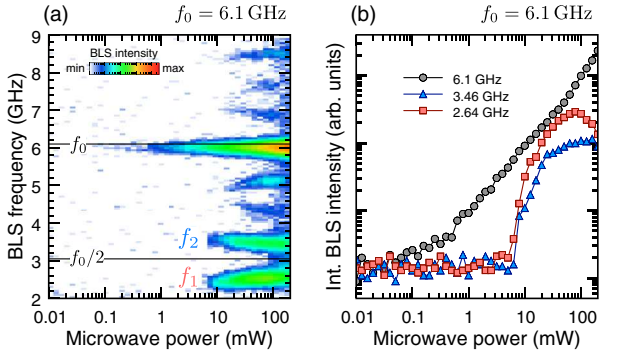

FIG. 3. (a) Power dependence of the BLS spectra excited at $f_0 = 6.1$ GHz. (b) BLS intensity integrated in 800-MHz wide frequency windows around the BLS frequencies $f_0 = 6.1$, $f_1 = 2.64$, and $f_2 = 3.46$ GHz as a function of the microwave power. In the double-logarithmic plot, the direct excitation at 6.1 GHz follows a linear trend, whereas the split modes at 3.46 and 2.64 GHz show a clear threshold behavior.

To further elucidate the threshold character of the 3-magnon splitting, we plot a more detailed power dependence of the magnon intensities in Fig. 3(a) for $f_0 = 6.1$ GHz. While the mode at 6.1 GHz can be observed over a large power range, it is evident that the split modes f_1 and f_2 only appear above a certain threshold power. Furthermore, we observe a pronounced frequency shift of these two split modes with increasing microwave power. For a quantitative comparison, we integrate the BLS intensity in narrow frequency windows around the directly and indirectly excited modes, respectively, and plot them in Fig. 3(b). The double logarithmic scale reveals the linear growth of the direct excitation at 6.1 GHz starting at 0.1 mW. However, the intensities of the satellite peaks around $f_1 = 2.65$ and $f_2 = 3.48$ GHz abruptly increase above 10 mW which demonstrates the threshold character of the splitting process.

In order to reveal the spatial structure of the modes that are generated via 3-magnon scattering, we simultaneously mapped the profiles of the directly excited mode and the split modes [Figs. 4(c)–4(g)]. Additionally, we compare the experimental results for the mode with highest intensity at 6.1 GHz with micromagnetic simulations [38] in Fig. 4(b) (for details please see Supplemental Material [24]). The first thing to realize is that all of the split modes show a clear azimuthal character and confirm the analytical calculations and the selection rules imposed by the rotational symmetry: pure radial modes with $(n, 0)$ split in modes with $m_1 = -m_2$ and $n_1 \neq n_2$. As far as possible, we label the modes according to their radial and azimuthal mode numbers (n, m). We resolve azimuthal mode numbers up

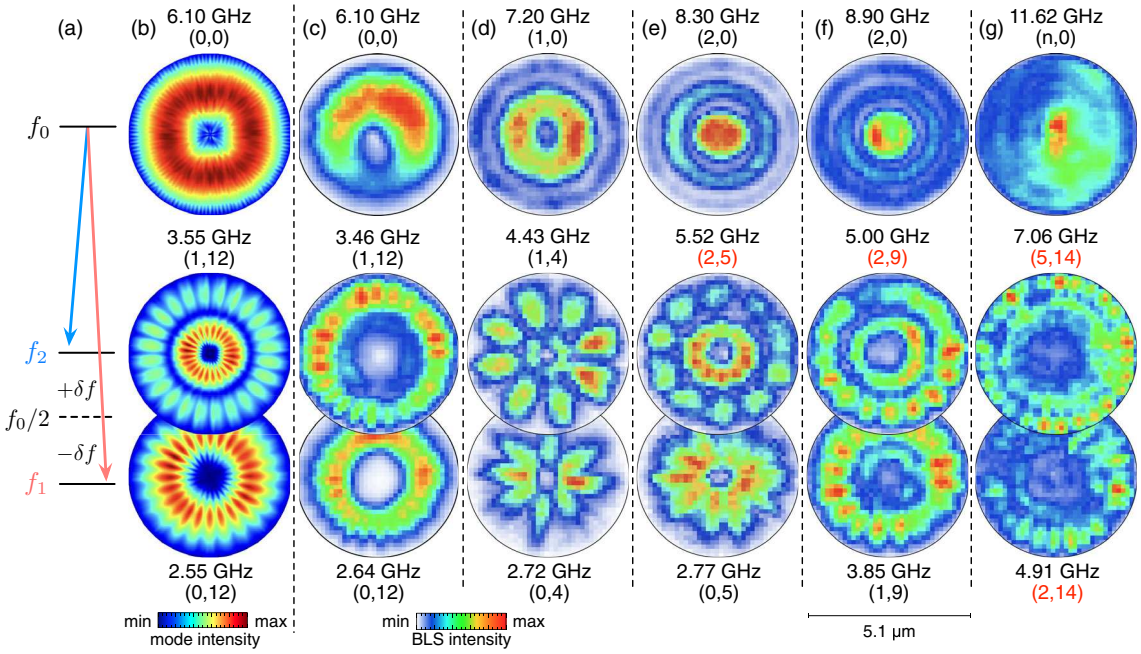

FIG. 4. (a) Energy levels for 3-magnon splitting. (b) Micromagnetic simulation of the 3-magnon splitting for the excitation frequency of 6.1 GHz. (c)–(g) Spatial intensity distributions of the direct excitation (upper line) as well as the split modes (middle and bottom line) for various excitation frequencies. Each magnon mode has been identified regarding its radial and azimuthal order (n, m). Numbers in red are derived by comparing the experimentally detected magnon frequency to analytical calculations [Fig. 1(b)].

to 14, to our knowledge the first time to observe vortex modes with such high m. For higher n, an unambiguous identification of the modes was not possible due to limited spatial resolution. However, the radial mode number can still be retrieved by comparing the measured frequencies to the analytic calculations in Fig. 1(b). We counted the azimuthal mode numbers and plotted the measured frequencies as black dots in the calculated spectrum. From this comparison we then determined the radial mode numbers (red labels in Fig. 4).

In Fig. 4(b), the micromagnetic simulation for excitation at 6.1 GHz reveals the splitting into magnons with the same mode numbers as in the experiment, however, with slightly different frequencies of the split modes. This frequency shift may be attributed to variations in the strength and symmetry of the exciting magnetic field or the material parameters. For further details please see Supplemental Material [24].

Note that we only measure stationary mode profiles which implies that, essentially, all split modes are a superposition of modes counterpropagating in the azimuthal direction. Therefore, we conclude that the two splitting processes $(n_0, 0) \rightarrow (n_1, m) + (n_2, -m)$ and $(n_0, 0) \rightarrow (n_1, -m) + (n_2, m)$ occur with equal probability.

It is remarkable, that the higher m for a given n, the stronger the mode is localized at the outer circumference of the disc, resembling intensity distributions of optical whispering gallery modes [39]. The most beautiful example in our dataset is the intensity distribution of the split mode (0,12) at the excitation frequency 6.1 GHz shown in Fig. 3(c). It exhibits a distinct area with zero intensity in its center, similar to higher order optical whispering gallery modes.

In summary, we shed light on the nonlinear conversion of magnons in a confined system with rotational symmetry by analyzing their spectral and spatial characteristics. We showed how this mechanism can be utilized to generate magnons with unprecedented high azimuthal wave vectors and localization at the discs' perimeter, which resembles the character of whispering gallery modes. The underlying 3-magnon scattering processes are highly tunable regarding the frequency and spatial distribution of the split modes. We believe that this advanced control of the generation of whispering gallery magnons is a missing link towards the realization of an efficient hybridization of magnons and other quantum particles as found in circular optical cavities and mechanical quantum resonators.

The authors acknowledge fruitful discussions with S. V. Kusminskiy. Financial support by the Deutsche Forschungsgemeinschaft is gratefully acknowledged within program SCHU2922/1-1. K. S. acknowledges funding within the Helmholtz Postdoc Programme. Samples were fabricated at the Nanofabrication Facilities (NanoFaRo) at the Institute of Ion Beam Physics and Materials Research at HZDR. We thank B. Scheumann for film deposition and L. Bischoff for the thickness measurement.

*Corresponding author.
k.schultheiss@hzdr.de

[1] G. Mie, Ann. Phys. (N.Y.) **330**, 377 (1908).
[2] P. Debye, Ann. Phys. (N.Y.) **335**, 755 (1909).
[3] L. Rayleigh, Philos. Mag. **27**, 100 (1914).
[4] A. N. Oraevsky, Quantum Electron. **32**, 377 (2002).
[5] K. J. Vahala, Nature (London) **424**, 839 (2003).
[6] Y. Tabuchi, S. Ishino, T. Ishikawa, R. Yamazaki, K. Usami, and Y. Nakamura, Phys. Rev. Lett. **113**, 083603 (2014).
[7] A. Osada, R. Hisatomi, A. Noguchi, Y. Tabuchi, R. Yamazaki, K. Usami, M. Sadgrove, R. Yalla, M. Nomura, and Y. Nakamura, Phys. Rev. Lett. **116**, 223601 (2016).
[8] J. A. Haigh, A. Nunnenkamp, A. J. Ramsay, and A. J. Ferguson, Phys. Rev. Lett. **117**, 133602 (2016).
[9] S. V. Kusminskiy, H. X. Tang, and F. Marquardt, Phys. Rev. A **94**, 033821 (2016).
[10] J. Graf, H. Pfeifer, F. Marquardt, and S. V. Kusminskiy, Phys. Rev. B **98**, 241406 (2018).
[11] X. Y. Zhang, C.-L. Zou, N. Zhu, F. Marquardt, L. Jiang, and H. X. Tang, Nat. Commun. **6**, 8914 (2015).
[12] H. Suhl, J. Phys. Chem. Solids **1**, 209 (1957).
[13] C. Ordonez-Romero, B. A. Kalinikos, P. Krivosik, W. Tong, P. Kabos, and C. E. Patton, Phys. Rev. B **79**, 144428 (2009).
[14] H. Schultheiss *et al.*, Phys. Rev. Lett. **103**, 157202 (2009).
[15] R. E. Camley, Phys. Rev. B **89**, 214402 (2014).
[16] T. Shinjo, T. Okuno, R. Hassdorf, K. Shigeto, and T. Ono, Science **289**, 930 (2000).
[17] V. Novosad, M. Grimsditch, K. Y. Guslienko, P. Vavassori, Y. Otani, and S. D. Bader, Phys. Rev. B **66**, 052407 (2002).
[18] K. Y. Guslienko and V. Novosad, J. Appl. Phys. **96**, 4451 (2004).
[19] V. Novosad, F. Y. Fradin, P. E. Roy, K. Buchanan, K. Y. Guslienko, and S. D. Bader, Phys. Rev. B **72**, 024455 (2005).
[20] K. Y. Guslienko, A. N. Slavin, V. Tiberkevich, and S.-K. Kim, Phys. Rev. Lett. **101**, 247203 (2008).
[21] M. Buess, R. Höllinger, T. Haug, K. Perzlmaier, U. Krey, D. Pescia, M. R. Scheinfein, D. Weiss, and C. H. Back, Phys. Rev. Lett. **93**, 077207 (2004).
[22] M. Buess, T. P. J. Knowles, R. Höllinger, T. Haug, U. Krey, D. Weiss, D. Pescia, M. R. Scheinfein, and C. H. Back, Phys. Rev. B **71**, 104415 (2005).
[23] B. A. Kalinikos and A. N. Slavin, J. Phys. C **19**, 7013 (1986).
[24] See Supplemental Material at http://link.aps.org/supplemental/10.1103/PhysRevLett.122.097202 for additional information on sample fabrication, the experimental technique of Brillouin light scattering and an introduction to the theoretical calculations.
[25] V. S. L'vov, *Wave Turbulence Under Parametric Excitation* (Springer-Verlag, New York, 1994).
[26] P. Krivosik and C. E. Patton, Phys. Rev. B **82**, 184428 (2010).
[27] K. Livesey, Nonlinear Behavior in Metallic Thin Films and Nanostructures, in *Handbook of Surface Science*, edited by R. E. Camley, Z. Celinski, and R. L. Stamps (Elsevier, North-Holland, 2015), Vol. 5.
[28] A. Yu. Galkin, B. A. Ivanov, and C. E. Zaspel, Phys. Rev. B **74**, 144419 (2006).
[29] K. Y. Guslienko and A. N. Slavin, J. Appl. Phys. **87**, 6337 (2000).
[30] R. Zivieri and F. Nizzoli, Phys. Rev. B **71**, 014411 (2005).
[31] A. A. Awad, G. R. Aranda, D. Dieleman, K. Y. Guslienko, G. N. Kakazei, B. A. Ivanov, and F. G. Aliev, Appl. Phys. Lett. **97**, 132501 (2010).
[32] B. Taurel, T. Valet, V. V. Naletov, N. Vukadinovic, G. deLoubens, and O. Klein, Phys. Rev. B **93**, 184427 (2016).
[33] T. Sebastian, K. Schultheiss, B. Obry, B. Hillebrands, and H. Schultheiss, Front. Phys. **3**, 35 (2015).
[34] K. Vogt, O. Sukhostavets, H. Schultheiss, B. Obry, P. Pirro, A. A. Serga, T. Sebastian, J. Gonzalez, K. Y. Guslienko, and B. Hillebrands, Phys. Rev. B **84**, 174401 (2011).
[35] H. Schultheiss, K. Vogt, and B. Hillebrands, Phys. Rev. B **86**, 054414 (2012).
[36] H. Suhl, J. Appl. Phys. **31**, 935 (1960).
[37] P. A. Praveen Janantha, B. Kalinikos, and M. Wu, Phys. Rev. B **95**, 064422 (2017).
[38] A. Vansteenkiste, J. Leliaert, M. Dvornik, M. Helsen, F. Garcia-Sanchez, and B. Van Waeyenberge, AIP Adv. **4**, 107133 (2014).
[39] J. J. Yang, M. Huang, J. Yu, and Y. Z. Lan, Europhys. Lett. **96**, 57003 (2011).